Cross-shelf transport, oxygen depletion, and nitrate release within a forming mesoscale eddy in the eastern Indian Ocean

Anya M. Waite, Lynnath E. Beckley, Lionel Guidi, Jason P. Landrum, David Holliday, Joseph Montoya, Harriet Paterson, Ming Feng, Peter A. Thompson, Eric J. Raes

LIMNOLOGY
and
OCEANOGRAPHY

ASLO

Limnol. Oceanogr. 00, 2015, 00–00

doi: 10.1002/lno.10218

Cross-shelf transport, oxygen depletion, and nitrate release within a forming mesoscale eddy in the eastern Indian Ocean

Anya M. Waite,[†*1] Lynnath E. Beckley,[2] Lionel Guidi,[3,4] Jason P. Landrum,[5,6] David Holliday,[2] Joseph Montoya,[5] Harriet Paterson,[1,7] Ming Feng,[8] Peter A. Thompson,[9] Eric J. Raes[1]

[1]The Oceans Institute and School of Civil, Environmental and Mining Engineering, The University of Western Australia, Crawley, WA, Australia
[2]Environmental and Conservation Sciences, School of Veterinary & Life Sciences, Murdoch University, Murdoch, WA, Australia
[3]Sorbonne Universités, UPMC Université Paris 06, CNRS, Laboratoire d'oceanographie de Villefranche (LOV), Observatoire Océanologique, Villefranche-sur-Mer, France
[4]Department of Oceanography, University of Hawaii, Honolulu, Hawaii, USA
[5]School of Biology, Georgia Institute of Technology, Atlanta, Georgia
[6]AAAS Overseas Fellow serving at the United States Agency for International Development, San Salvador, El Salvador
[7]Centre of Excellence in Natural Resource Management, The University of Western Australia, Albany, WA, Australia
[8]Commonwealth Scientific and Industrial Research Organisation, Centre for Environment and Life Sciences, Floreat, WA, Australia
[9]CSIRO Oceans & Atmosphere, Hobart, Tasmania, Australia

Abstract

Mesoscale eddies may drive a significant component of cross-shelf transport important in the ecology of shelf ecosystems and adjacent boundary currents. The Leeuwin Current in the eastern Indian Ocean becomes unstable in the austral autumn triggering the formation of eddies. We hypothesized that eddy formation represented the major driver of cross-shelf transport during the autumn. Acoustic Doppler Current Profiler profiles confirmed periodic offshore movement of ~2 Sv of shelf waters into the forming eddy from the shelf, carrying a load of organic particles (>0.06 mm). The gap between inflow and outflow then closed, such that the eddy became isolated from further direct input of shelf waters. Drifter tracks supported an anticyclonic surface flow peaking at the eddy perimeter and decreasing in velocity at the eddy center. Oxygen and nutrient profiles suggested rapid remineralization of nitrate mid-depth in the isolated water mass as it rotated, with a total drawdown of oxygen of 3.6 mol m^{-2} to 350 m. Depletion of oxygen, and release of nitrate, occurred on the timescale of ~1 week. We suggest that N supply and N turnover are rapid in this system, such that nitrate is acting primarily as a regenerated nutrient rather than as a source of new nitrogen. We hypothesize that sources of eddy particulate C and N could include particles sourced from coastal primary producers within ~500 km such as macrophytes and seagrasses known to produce copious detritus, which is prone to resuspension and offshore transport.

Introduction

Recent work has highlighted the importance of mesoscale eddies (~100 km) in driving vertical nutrient fluxes and primary production globally (Chelton et al. 2011), with important regional hot-spots (Rodriguez et al. 2001; Baltar et al. 2010; Painter et al. 2010). Such dynamic features can also drive a significant component of cross-shelf transport important in the ecology of coastal ecosystems (Holliday et al. 2012). Interactions between continental shelf and boundary currents, can induce large-scale cross-shelf water movements (Csanady 1997; Werner and Quinlan 2002). These interactions involve a range of meanders, eddies, and upwelling features important in driving cross-shelf exchange of nutrients and biota (Heath 1992; Csanady 1997). The key challenge for investigators has been the integration of process understanding across the very different temporal and spatial scales occurring for shelf and offshore processes (Csanady 1997).

[†]Present address: Alfred Wegener Institute for Polar and Marine Research, Bremerhaven, Germany and Universität Bremen, Bremen, Germany

Additional Supporting Information may be found in the online version of this article.

*Correspondence: anya.waite@awi.de

From the coastal perspective, eddies as drivers of advective loss of shelf water and biota have been described for several boundary current systems, (e.g., Heath 1992; Nakata et al. 2000). Rapid cross-shelf exchange in the mid-Atlantic Bight results from warm-core eddies (rings) interacting with shelf water at the shelf-slope front (Cowen et al. 1993). There, propagation of eddies along the continental shelf induces advection and entrainment of shelf water to eddy peripheries via "streamers" or filaments. Recent investigations of Haida eddies in the Alaska Current also identified the presence of coastal-derived nutrients and modified shelf phytoplankton and zooplankton communities (Myers and Drinkwater 1989; Mackas et al. 2005; Ladd et al. 2009). In the south eastern Indian Ocean off Western Australia, the local boundary current the Leeuwin Current (LC) hosts fish populations vulnerable to offshore larval losses (Gaughan 2007; Holliday et al. 2012) making cross-shelf transport also a potential loss term for coastal populations.

The shelf and offshore regions of the south eastern Indian Ocean are more oligotrophic than other eastern boundary systems, such that export of moderate concentrations of coastal nutrients has a major impact on offshore foodwebs and productivity (Waite et al. 2007a). Anticyclonic (warm-core) eddies of the LC can contain coastal diatoms growing well seaward of the shelf break (Thompson et al. 2007). Waite et al. (2007a,b) hypothesized that innocula of coastal diatoms and/or their nutrient sources were incorporated during eddy formation, possibly via cross-shelf mixing between shelf and LC waters (Feng et al., 2007). Paterson et al. (2008) determined that forming eddies on the shelf-break have sufficient concentration of nutrients to drive such blooms as the eddies mature. However, to date no data existed detailed enough to test these hypotheses.

Here, we present a detailed investigation of cross-shelf transport during formation of a large mesoscale eddy in the eastern Indian Ocean. We argue that the eddy itself is the essential mixing crucible for the locally high production documented in warm core eddies off Western Australia, and that the eddy formation process represents the major driver of cross-shelf transport during the autumn. We use conductivity–temperature–depth (CTD) transects, SeaSoar transects, and Lagrangian surface drifters to investigate mixing water masses during eddy formation, and conclude that, while local phytoplankton sources provide significant chlorophyll *a* (Chl *a*) to the eddy during formation, particles from other sources are likely to be important. We estimate the time scales of oxygen depletion and associated nutrient release. The eddy drives significant biogeochemical transformations important in modifying offshore nutrient budgets and ecosystem structure.

Materials and methods

Study area and data collection

The formation of an anticyclonic eddy of the LC, located west of Rottnest Island off Western Australia, was investigated over a 25 d period during May 2006 on the RV Southern Surveyor. Eddies are a recurrent, but not permanent feature of the LC, so sampling was planned for the period of formation during the autumn intensification of the LC (Cresswell 1991; Pearce 1991). The operational area was from 30°S–34°S and up to 370 km (112°E) offshore of the southwestern Australian coast (Paterson et al. 2008; Fig. 1). The evolution of the anticyclonic eddy off the Perth Canyon was followed for the weeks prior to the cruise using remotely sensed sea surface temperature (SST) and sea surface height anomaly data (Paterson et al. 2008, 2013).

Along the ship track, continuous underway measurement of the horizontal current velocity field along the ships track was obtained using a vessel mounted RDI 70 kHz Ocean Surveyor Acoustic Doppler Current Profiler (ADCP) (Teledyne RD Instruments). The instrument was set to record from just below the surface to a maximum water column depth of 300 m and data were averaged in 8 m depth bins.

Between 02 May and 27 May, 120 CTD casts were performed across the eddy and in adjacent water masses using a Seabird SBE 911 Plus instrument with dual temperature and conductivity sensors and a Chelsea TGI fluorometer attached to a 24 × 10 L-bottle Niskin rosette. Maximum cast depth was to 500 m or to within 10 m of the bottom in shallower water. For some locations, CTD casts were performed to 1000 m. The rosette system carried a Wetlabs C-Star^{TM} transmissometer, a Seabird dissolved oxygen sensor (SBE43) and transmissometer, used here as an indicator of fine particle concentration (Karageorgis et al. 2008). Of the 120 CTD casts, 18 were primary production stations including measurements of particulate organic carbon (POC) and particulate nitrogen (PN), and ^{13}C carbon uptake (see below).

Underwater particles (>60 μm), which include phytoplankton chains and aggregates, detrital particles, and some zooplankton, were enumerated in situ using the Underwater Vision Profiler 4 (UVP4) (Picheral et al. 2010). The UVP recorded images every 8 cm. To avoid light contamination, images deeper than 40 m were used for day profiles. Objects in each image were detected, sized, and enumerated on custom software (Picheral et al. 2010) based on the lateral scattering of light from a particle. Total number of pixels is converted to Equivalent Spherical Diameter. We present the data for small particles 60–550 μm. as volumetric particle concentrations (# L^{-1}) or as biovolume/water volume (ppm). Particle biovolume was converted to C content of large particles using the equations in Guidi et al. (2008). We executed UVP casts to 1000 m or maximum depth. We also executed one high-resolution UVP transect along the N–S 113.32°E line over 36 h on 22–23 May (Fig. 1E). CTD drops (as above) to 500 m were executed every ~20 km along this line; UVP drops were made to 1000 m.

Chl *a* measurements were made via filtration of 1 L of water (from up to 10 depths) on to GF/F filters and analyzed at sea (Parsons et al. 1984). Dissolved inorganic nitrate (Nitrate and Nitrite, hereafter Nitrate) was analyzed for all depths using Quick-Chem^{TM} methods on a flow injection

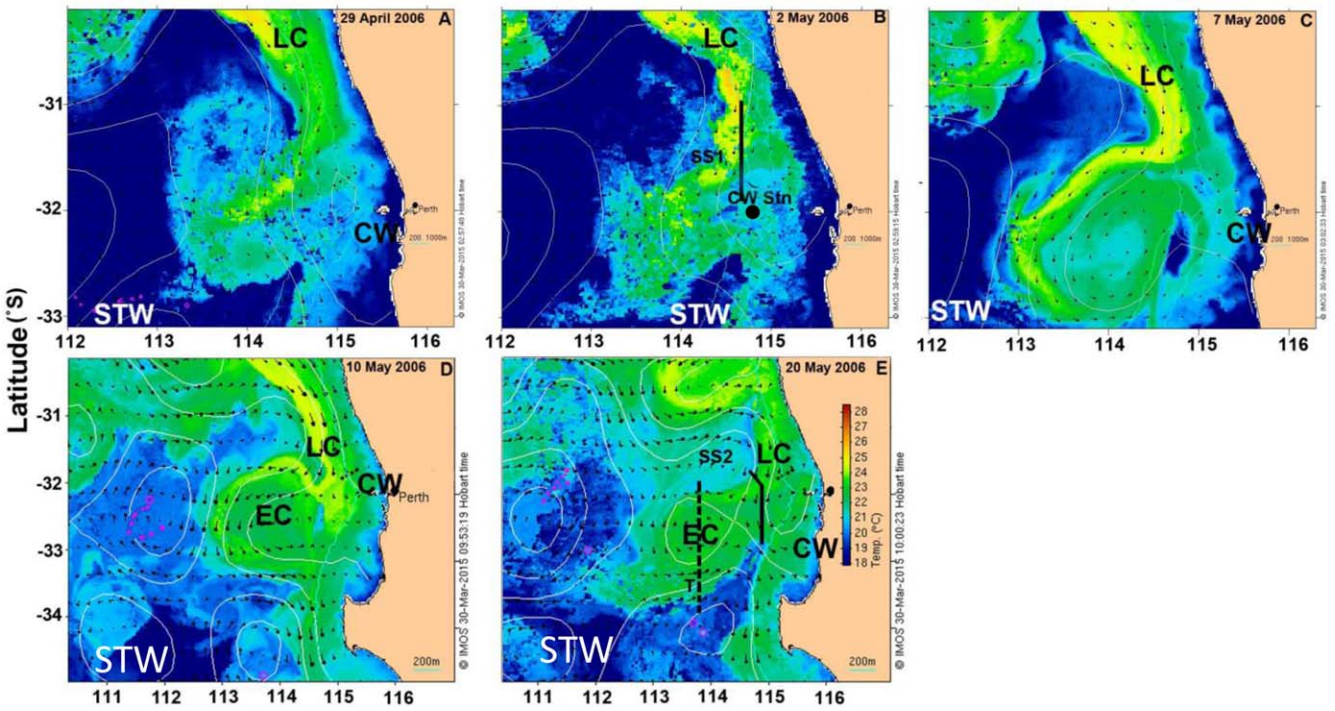

Fig. 1. Sea-surface temperature (MODIS) showing the Leeuwin Current flowing southward along the shelf break during the early formation of the eddy (Period 1). Black line represents Sea Soar 1 (SS1). (**A**–**D**), and late eddy formation (Period 2) (**E**). (**A**) 29 April. (**B**) 3 May, black dot indicates location of continental shelf waters (CW) station. (**C**) By 7th May the meander had begun to close, with the southern arm of the meander meeting the northern arm of the meander in a mushroom shape. (**D**) By 10th May the meander had almost closed, such that by the 14th of May the eddy center was isolated from the coast. (**E**) By 20 May the eddy was circulating independently from the LC, which had begun to flow again contiguously along the 200 m contour. Black line represents Sea Soar 2 (SS2); dashed line shows N-S CTD transect. For all panels, CW = Continental Shelf Waters, STW = Subtropical Surface Waters, LC = Leeuwin Current, and EC = Eddy Centre.

LACHAT® instrument as per the following protocols for nitrate + nitrite (Quik-Chem™ Method 31-107-04-1-A; detection limit ~0.03 μmol L^{-1}; adapted from Wood et al. 1967). Dissolved oxygen concentrations from each bottle sample were also measured by automated Winkler titration on a Metrohm 765 Dosimat™. SBE 43 electrode data were compared with chemically measured values via standard MNF protocols.

Primary production and POC and nitrogen

Water samples were collected every 3 d along the drifter tracks (see below) for measurement of carbon fixation rates within the water column. Samples were collected at night via a CTD-rosette system at the surface, the deep chlorophyll maximum, and below the chlorophyll maximum. Water was held in black carboys at 4°C until the water was used in experiments at dawn. Before dawn (~0500 local time), samples were transferred to 4-L polycarbonate incubation bottles equipped with a silicone septum cap. After filling the bottles with water, trace amounts of $H^{13}CO_3$ (99 atom%, Cambridge Isotope) were added to each bottle with gas tight syringes. At dawn, experimental bottles were placed in acrylic incubators fitted with a flow-through seawater system. Bottles were shaded with individual neutral-density mesh bags to stimulate in situ light conditions for phytoplankton collected at various depths. Experimental bottles containing surface water were exposed to full sunlight. All experiments ran for 24 h and were terminated via filtration through a low-pressure (i.e., <10 psi) filtration on to 25 mm precombusted GF/F filters (~0.7 μm pore size). Filters were folded into centrifuge tubes and frozen at −80°C until the end of the voyage. Ashore, all filters were dried at 60°C, fumed with concentrated HCl to remove carbonates, and analyzed for isotopic composition via continuous-flow isotope ratio mass spectrometry using a Carlo Erba NC 2500 elemental analyzer coupled to a Micromass Optima mass spectrometer. We conservatively estimate that the overall analytical precision of our isotopic measurements is $\pm 0.1‰$. Comparison of POC and PN concentrations between water masses were executed via analysis of variance with water masses as the variable ANOVA (Sigmaplot® v13). CO_2-fixation rates were calculated using a similar isotope mass balance approach as described by Montoya et al. (1996) and applied in similar field experiments by Holl et al. (2007) where the ambient concentration of dissolved inorganic carbon was based on the in situ salinity and temperature of the water collected and used in our experiments at each station (Parsons et al. 1984). Vertically integrated CO_2-fixation rates were estimated for each station, and were calculated via trapezoidal integration with depth.

Table 1. Surface layer properties of the primary water masses encountered in the study, including temperature, particulate matter, and dissolved nutrient concentrations. Shaded cells in dark grey are data averaged across all regional CTD measurements at end points of regional T-S plot, where LC = the warmest, least saline water mass, and STW = the highest salinity waters, regionally. Pale grey cells denote averages of surface water mass characteristics from 1 to 2 CTD casts, limited to the mixing line between LC and STW and thus restricted to surface waters. For integrated values, *N* refers to measurements at replicate stations, defined as a minimum of two individual CTD casts within 10 km of each other in a similar water mass as defined by TS properties. Numbers in brackets indicate standard deviation. Identical superscripts indicate statistically similar values across a row, for surface particulate organic carbon (POC) and surface particular nitrogen (PN) only.

	Leeuwin current (LC)	*N*	Subtropical waters (STW)	*N*	Coastal water (CW)	*N*	Eddy center (EC)	*N*
Temperature °C	22.78 (0.45)	2485	19.57 (0.49)	3484	21.93 (0.07)	830	22.06 (0.46)	2025
Salinity psu	35.39 (0.04)	2485	35.91 (0.03)	3484	35.61 (0.02)	830	35.52 (0.10)	2025
Surface POC (mg m^{-3})	3.05*† (0.68)	4	2.37* (0.11)	4	3.96† (0.38)	3	4.29† (0.15)	2
Surface PN (mg m^{-3})	0.361* (0.066)	4	0.340* (0.019)	4	0.637† (0.102)	3	0.675† (0.015)	2
Integrated POC to 150 m (mg m^{-2})	5343 (938)	2	3801	1	4032 (1844)	3	5835	1
Integrated PN to 150 m (mg m^{-2})	670 (24)	2	660	1	732 (383)	3	1051	1
Nitrate to 150 m (mmol m^{-2})	72 (50)	2	42	1	72 (35)	3	140	1
PN + Nitrate to 150 m (mmol m^{-2})	105 (0.41)	2	89	1	124 (47)	3	215	1
Silicate to 150 m (mmol m^{-2})	436 (40)	2	253	1	466 (214)	3	411	1
Large Particle POC to 150 m ($>$ 20 μm, mg m^{-2})	402 (43)	2	296	1	1190 (414)	2	549	1
Large Particle UVP Biovolume $>$ 60 μm (mm^3 m^{-2})	43.3 (94)	2	12	1	99.6	1	67.9	1

Note: *$p<0.05$

To determine regional correlates with oxygen concentrations, multiple linear regression on untransformed oxygen, transmission, salinity, temperature, latitude, and longitude, using the regression package associated with Sigmaplot® v13.

Surface-drifting buoys

Circulation of the LC and anticyclonic eddy was examined using two Iridium satellite-tracked, surface-drifting buoys (Fastwave Communications Pty Ltd). Each drifter was equipped with two sediment trap arrays, and 40 kg bar-bell weights at 245 m. This system has been shown to be effective in reflecting circulation within the upper mixed layer while minimizing influence of surface wind-driven transport (Nodder and Waite 2001; Nodder et al. 2001). Drifters were set to report positions at 5 min intervals with an accuracy of 10 m.

Drifter 1 was deployed on 05 May 2006 within the LC north and slightly upstream of the meander (114° 39.97′ E, 31° 0.072′ S). Drifter 2 was deployed to define the rotational circulation and current velocities within the eddy, (1) just within the eddy perimeter and (2) near the eddy center. The first deployment of drifter 2 was undertaken in the southeast margin of the eddy (113° 45.36′ E, 32° 50.098′ S) on 07 May. The second deployment of drifter 2 was close to the eddy center at 113° 32.60′ E, 32° 48.708′ S on 20 May. All drifters were retrieved and redeployed at 3 d intervals during which time full sampling at these locations was performed. Drifters were redeployed at the approximate position of retrieval.

SeaSoar transects

A modified SeaSoar (Waite et al. 2007b) was used to generate two snapshots of shelf-break water column structure, one before SeaSoar 1 (SS1) and one after SeaSoar 2 (SS2) the eddy had closed off from contact with the shelf. Sensors included temperature, salinity, turbidity, oxygen, and fluorescence.

Results

Evolution of forming eddy

We used IMOS Ocean Current SST images to estimate the time scale for the initiation and closure of the meander

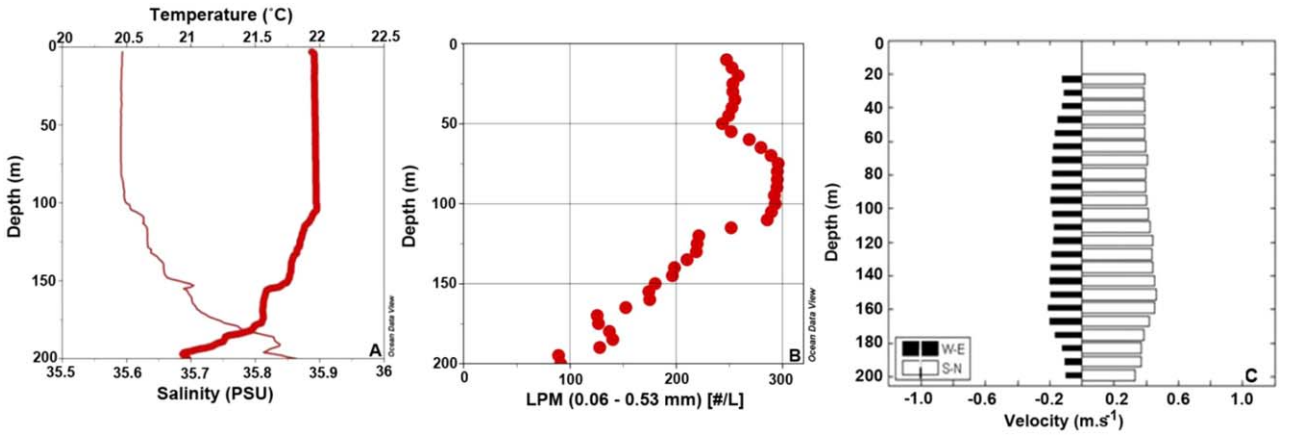

Fig. 2. Vertical profile of water properties of continental shelf waters (CW) (position shown as black dot, Fig. 1B) on 3rd May at the 1000 m contour. (**A**) Physical properties, temperature (bold line), and salinity (normal line) suggested the mixed layer was well mixed below 100 m. (**B**) Large Particle concentrations (0.06–0.53 mm); in # L^{-1} measured by the UVP indicate a particle maximum within the mixed layer at 75–120 m which was being advected offshore. (**C**) ADCP profiles indicate the CW water mass was flowing directly into the center of the meander, moving *N* at 0.4 m s^{-1} and W at 0.2 m s^{-1}, i.e., NNW at ~0.44 m s^{-1}. [Color figure can be viewed in the online issue, which is available at wileyonlinelibrary.com.]

(Period 1) for offshore flux calculations. We used an ADCP, UVP particle estimates, as well as POC and PN measurements from the Continental Shelf Water (CW) CTD cast and SS1 to estimate the offshore velocities and fluxes of nitrogen, carbon, and Chl *a* during Period 1. A weak LC instability is visible in SST data at 32°S as early as mid-April, and the LC meander was fully visible by ~29 April (Fig. 1A), and shelf waters were flowing directly into the center of the meander (Fig. 1B) thereafter. The meander then curled northward, almost closing shoreward gap (Fig. 1C,D), but the opening toward the shelf persisted until ~14 May, making this the end of Period 1.

After 14 May, (Period 2) the meander was closed on the landward side (Fig. 1E), and the northern arm of the meander flowing offshore had met the southern arm of the meander as it returned shoreward, closing the center of the eddy off from direct connection with the shelf. Once closure of the meander isolated the eddy center, we used drifter tracks, and ADCP data to estimate the time and space scales of eddy rotation at three different distances from the eddy center. We made four separate estimates of oxygen depletion and nitrate release within the eddy based on (1) SeaSoar2 data, (2) CTD/UVP time series data along the drifter tracks (including particles, POC/PN, chlorophyll, dissolved nutrients, and oxygen) to estimate the rates of oxygen depletion and nitrate release within the eddy, (3) N–S CTD/UVP transect through the center of the eddy, and (4) pooled nitrate and oxygen data across the whole dataset.

Water mass characterization

As the properties of the LC and Subtropical Surface Waters (STW) can vary with season, year, and latitude, we characterized these two primary water masses from the temperature–salinity (TS) plot of all stations sampled; the LC was the warmest water sampled, at the apex of the TS plot, and STW were the most saline waters sampled (Supporting Information Appendix 1); summary statistics appear in Table 1. In TS space, CW and surface Eddy Center waters (EC) occurred in the mixing zone between LC and STW. Their boundaries were spatially determined; EC waters were sampled solely in Period 2, at the deepest pycnocline depth within the eddy center, while CW were a combination of Period 1 and Period 2 waters on the continental shelf in waters shallower than 1000 m. All particulate carbon and nitrogen concentrations were characterized by up to three production stations (Table 1).

The LC, sampled upstream of the meander at two stations in Period 1, showed warm temperatures (22.78°C) and low salinity (35.39 psu) typical for this time of year, with relatively high silicate and nitrate values (Table 1) and chlorophyll accumulation of 50 mg m^{-2}, indicating local autumn bloom conditions. PN values were statistically similar to those in STW (below) and significantly lower than in CW or the Eddy Center (EC); Table 1.

Subtropical Waters (STW) originate offshore in the Indian Ocean, and are more saline (35.91 psu) and cool (19.57°); they often subduct as a layer 100–200 m thick beneath the LC and slowly mix with it, making the LC more saline as it flows south (Feng et al. 2009). In our study these waters had the lowest particle concentrations regionally, and surface POC and PN concentrations, were statistically lower than CW and EC waters (Table 1).

CW were sampled at the shelf break in the center of offshore flow during Period 1, and slightly eastward of this in Period 2. Based on a simple salinity analysis, we suggest that CW injected into the eddy center was composed of ~half STW, ~half LC and was therefore likely to be "modified Leeuwin Current" water resulting from mixing between the

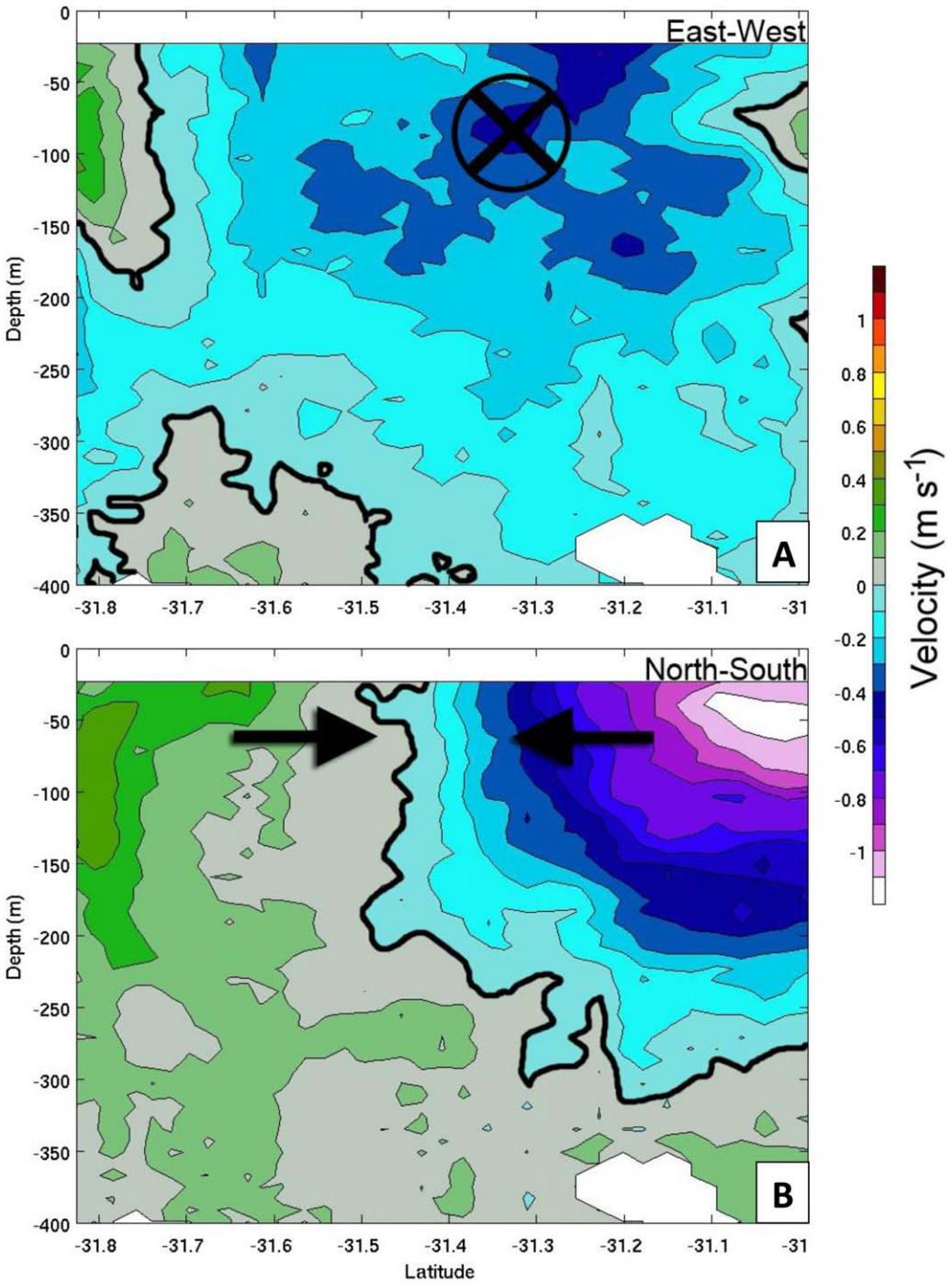

Fig. 3. SeaSoar transect 1 (SS1) across coastal waters (CW) flowing directly offshore along a N–S line adjacent to Stn1 (Fig. 1B). (**A**) ADCP profiles with eastward (red–orange–green) and westward (blue–purple) velocities showing core flux of CW moving westward offshore (labelled with "X") into the center of the meander for most of the length of the transect. (**B**) ADCP profiles of southward (blue–purple) and northward (red–orange–green) velocities across the SeaSoar transect indicating that the two arms of the meander are pinching together at the landward side of the eddy.

LC and near-shore waters over a period of weeks, during which chlorophyll concentrations can increase through near-shore primary production (Holliday et al. 2011). Of note were the especially high large particle (UVP) concentrations in the CW (Fig. 2B), which were almost double any other water mass, as well as very high carbon concentrations in the >20 μm size POC fraction (Table 1).

The Eddy Center (EC), sampled in Period 2 only, showed some regional anomalies including high concentrations (here PN + nitrate) over 200 mmol m^{-2} which is almost

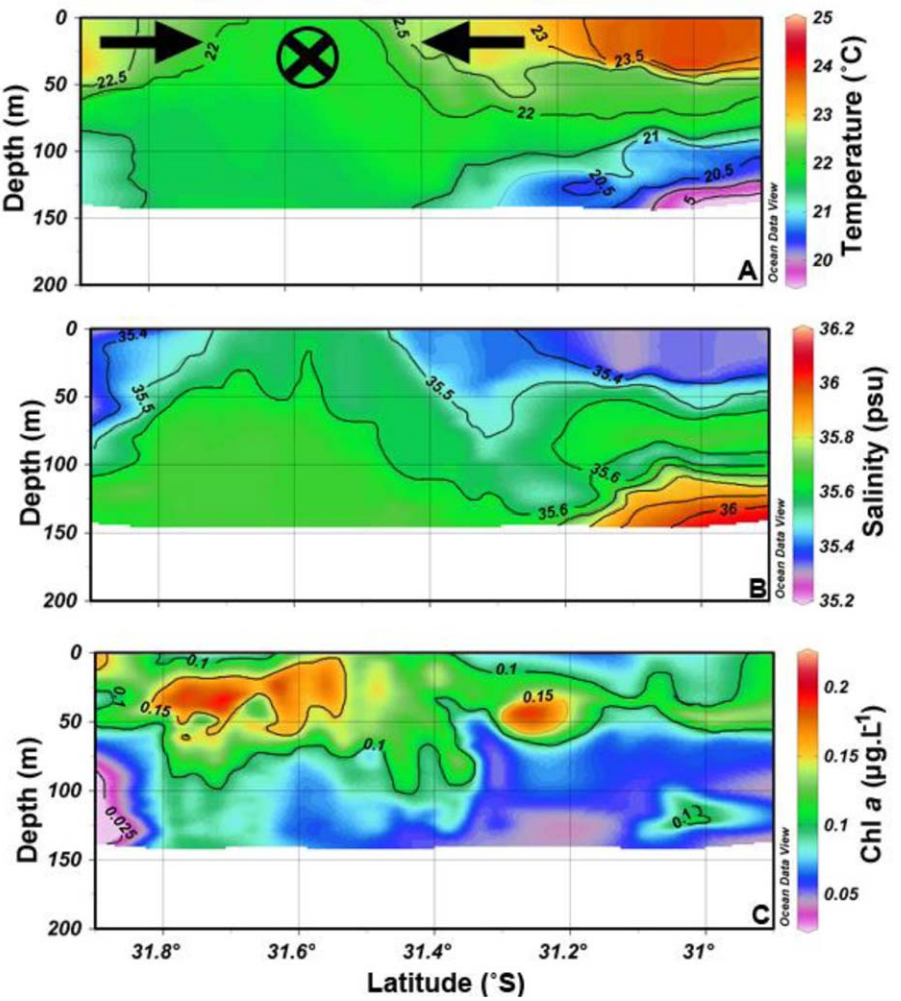

Fig. 4. SeaSoar1 (as in Fig. 1B). (**A**) Temperature (°C) on SS1. "X" represents core of (westward) offshore flow as measured by ADCP (Fig. 3) and solid arrows represent N–S ADCP vectors from Fig. 3. Note well-mixed central section of CW (31.4–31.8°S) moving offshore as less saline, warm LC waters pinch together on the landward side of the meander. (**B**) Salinity (psu) on SS1. (**C**) Fluorescence signal shows locally high concentrations of chlorophyll moving offshore between 31.4°S and 31.8°S. Leeuwin Current (LC) waters (north, right of figure) maintain a deeper fluorescence maximum.

double that of any potential source water mass (Table 1). Surface PN was statistically higher than in the LC or STW, but similar to that of CW.

The large particle concentrations measured as biovolume > 60 μm (UVP) and integrated with depth (Table 1) were strongly correlated with filtered carbon concentrations > 20 μm ($n = 11$, $p < 0.001$, $r^2 = 0.794$; Supporting Information Appendix 2). The fitted least squares relationship was: Biovolume ($mm^3\ m^{-2}$) = 0.098 × [Carbon (mg C m^{-2})] + 4.23.

Period 1—open meander: CW station and SS1

CW were sampled at a CTD station on the shelf break 1000 m contour (black dot, Fig. 1B). The water column was relatively well mixed to ~100 m (Fig. 2A) and a significant load large particles (>60 μm) peaked at 300 particles L^{-1} in at 100 m (Fig. 2B). ADCP data indicated that the water was flowing strongly offshore (~0.44 m s^{-1}) carrying this biogeochemical load in a north-northwesterly direction into the center of the eddy (Fig. 2C). These waters also carried moderately high Chl *a* concentrations (up to 0.55 μg L^{-1}), nitrate concentrations (0.1–0.8 μmol L^{-1}), and silicate concentrations (~2.5 μmol L^{-1}) (*see* also CW, Table 1).

SeaSoar1 (SS1; 5th May) transected CW flowing offshore in Period 1, 2 d after the CTD station above, while the center of the meander was still contiguous with the coastal shelf water mass (Fig. 1B). SS1 was executed from S to N through the westward flow of CW across the shelf into the center of the forming eddy (30° 58.9′ S 114° 40.2′ E to 31° 49.40′ S 114° 40.2′ E), on 5th May while the main flow of the LC formed a meander which was still open on the eastern side

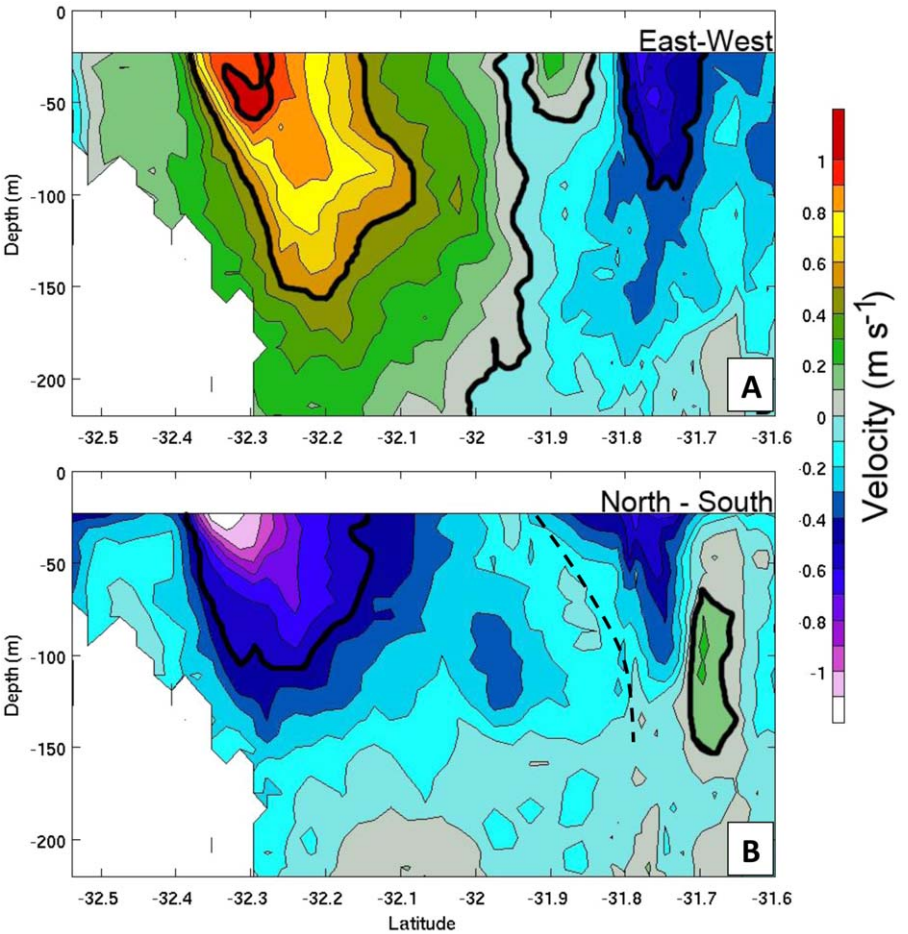

Fig. 5. SeaSoar 2 transect (SS2) (**A**) ADCP profiles show associated E–W subsurface flow field (Eastward = red and Westward = blue); Dashed line drawn by eye indicates the rough position of front between westward flowing and eastward flowing arms of the meander as indicated in the biogeochemical properties shown in Fig. 6. (**B**) ADCP profiles showing subsurface N/S velocities (Northward = blue and Southward = Red-green) show that both arms of the meander have a northward component of flow.

to the continental shelf. The ADCP measurements show that the shelf water transected by SS1 was still moving offshore across a region about 40 km wide, with a westerly velocity of 0.3–0.4 m s^{-1} (Fig. 3A) and the two arms of the meander north and south of this water mass were moving meridionally (N–S) toward each other, the northern arm of the LC moving south at up to 1 m s^{-1}, and the southern arm moving north at up to 0.3 m s^{-1} (Fig. 3B), suggesting that the two arms of the meander were drawing together; these high N–S velocities presaged the subsequent closure of the meander.

In the northern arm of the meander measured via SS1, LC waters were strongly stratified with warm surface temperatures (right-hand top of Fig. 4A), and low salinity (right-hand top of Fig. 4B) typical of the LC. Between the arms of the meander, temperature, salinity, and chlorophyll in CW were more well-mixed over the top 100 m (Fig. 4A–C). Chlorophyll fluorescence was relatively low (~0.1 μg L^{-1}) in LC water entering the northern side of the meander, with a narrow subsurface fluorescence maximum of 0.15 μg L^{-1} at ~45 m (Fig. 4C). The central CW mass flowing offshore showed a broader subsurface fluorescence peak between 10 m and 60 m throughout.

Period 2—closed meander: SS2 and N–S CTD transect

By 14th May the north and south arms of the meander had met, forming a strong front in both velocity (SS2; Fig. 5A,B), and water mass properties (SS2; Fig. 6A–C) as the meander closed on the shoreward (eastern) side. SS2 (21st May) was thus conducted after the LC meander had closed off from direct contact with the shelf waters (Paterson et al. 2008). SS2 was executed SE to NW across the two arms of the LC meander flowing offshore in the N and onshore in the S of the domain (Fig. 1D). Flows offshore in the north arm of the meander were due northwest at 0.84 m s^{-1}, while the onshore flows in the (now adjacent) south arm of the meander reached 1.49 m s^{-1}, almost due northeast, thus at ~90° to the northern meander. The complexity of the flow is simplified by superimposing the frontal line visible from the

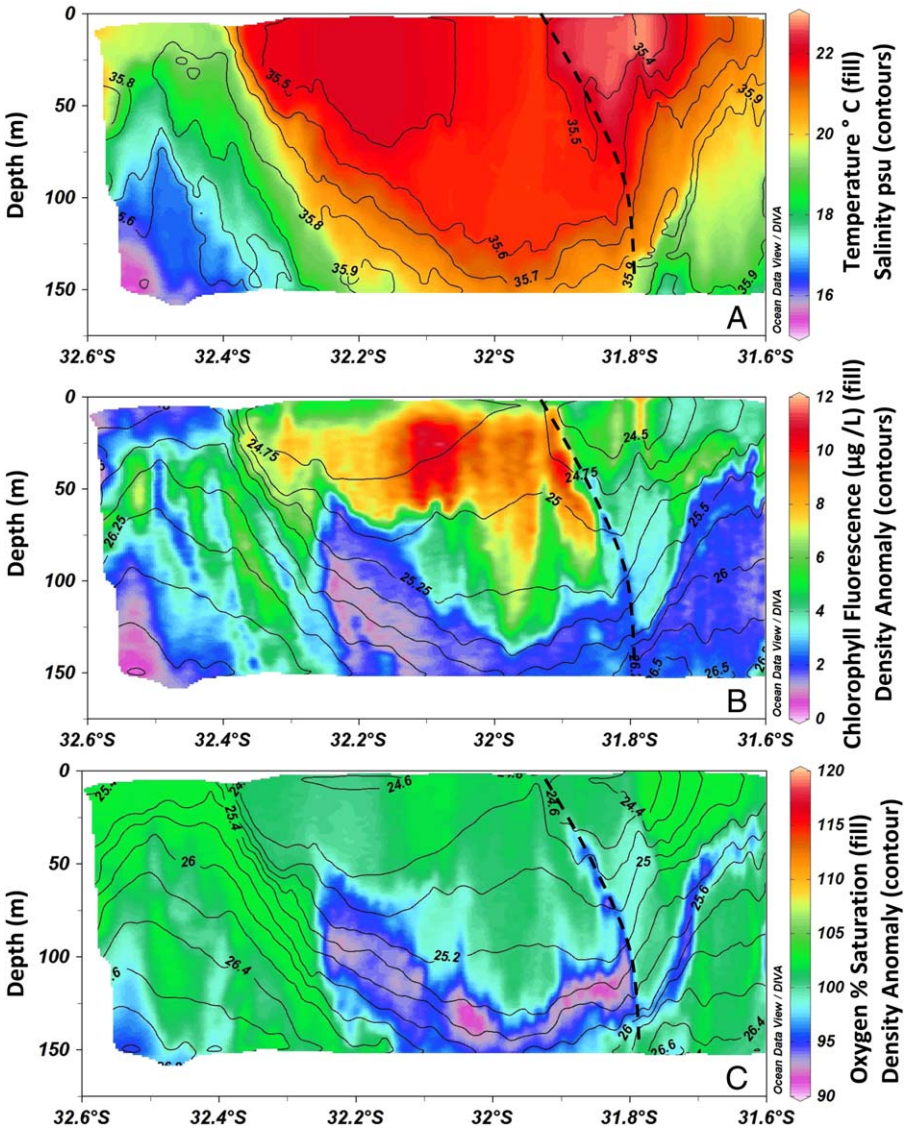

Fig. 6. SeaSoar2; ADCP properties of transect shown in Fig. 5. Dashed lines in each panel drawn by eye along the front separating the arms of the meander and indicates boundary between offshore-flowing waters of the meander to the north, and shoreward flow to the south consistent with ADCP data. (**A**) Temperature in deg. Celsius in colour fill, Salinity is given in black contours; (**B**) Fluorescence as a proxy for Chl *a* with calibration values given as μg Chl *a*/L. (**C**) Oxygen as % saturation, with density anomaly as black contour.

biogeochemical signatures (Fig. 6A–C; dashed black lines) as a region of minimum velocity between the NW and NE flow (dashed black line, Fig. 5B); this indicates the subsurface expression of the front between onshore and offshore flow which is discernable on the surface ADCP signatures).

We can then compare the water properties in the northern arm of the meander with the return flow ~7 d later (Fig. 6A–C; for time estimate of the rotation, see drifter tracks below). Offshore flow was more stratified (in both temperature and chlorophyll; Fig.6A,B), with higher oxygen concentrations (Fig. 6C) than the returning onshore flow. The shoreward flow in the south arm of the meander was twofold to threefold higher in Chl *a* than the northern offshore flow, much lower in transmission (not shown), slightly cooler (Fig. 6A), and slightly more saline at the surface. Between 80 m and 150 m, oxygen was significantly depleted in the shoreward return flow in comparison to the seaward flowing side of the meander (Fig. 6C). The return flow had particularly low oxygen concentrations immediately around the $\rho = 25.5$ density interface (Fig. 6C).

The N–S CTD transect crossed through the eddy center in Period 2 (Figs. 1E, 7A–D). Subtropical Waters (STW) formed a layer of high salinity under the CW in the center of eddy, with the highest salinities contiguous with the 20°C isotherm (Fig. 7A). Biogeochemical measurements indicated a spatial coherence of high nitrate and low oxygen signatures

within the center of the eddy (Fig. 7B,C), with oxygen depletion and nitrate release most extreme in the eddy center. Particle concentrations were highest in two layers, (1) within the mixed layer, and (2) in a clear maximum between the isopycnals $\rho = 25$ and $\rho = 25.5$ between 200 m and 300 m depth, just above the nitrate maximum (Fig. 7D, see $[NO_3] = 2$ μmol L^{-1}, Fig. 7B). These were also concentrated toward the center of the eddy. Isopycnals within the eddy were deflected downward to at least 1000 m depth.

Patterns in oxygen depletion emerging from complete dataset (Periods 1 and 2)

Multiple regression analysis on untransformed oxygen electrode data throughout the dataset elucidated variables that independently contributed to the variation in oxygen, indicating that longitude, salinity, and transmission were independent predictors of equal statistical weight (all parameters significant ($p < 0.001$)). Data were not normally distributed, nor were variances homogeneous. We examined individual regression plots to confirm that there were no extreme outliers driving the regressions. The F ratio used in the ANOVA (or regression analysis) has been shown to be very robust to departures from normality (Eisenhart 1947), and (Box 1953; Box 1962) showed that most hypothesis tests are reasonably robust against heterogeneity of variance. A threefold difference in variances does not affect the probability of a Type I error. But most tests of equality of variances are very sensitive to departures from the assumptions and usually do not provide a good basis for deciding to proceed with hypothesis tests (Box 1953). Minor deviations in homogeneity of variance and normality are therefore not a major concern in this application, as we are not specifically predicting O_2 from longitude or particle abundance or salinity. Instead, we are exploring the nature of these relationships to understand whether distance from shore (longitude) is related to O_2 independently of particle concentration and salinity. Oxygen concentrations were lowest in waters of relatively low salinity (therefore possibly associated with intrusions of LC waters), close to shore, where there were high particle concentrations (i.e., low transmission) (Table 2). The relationship was strongest between 150 m and 250 m depths, where salinity, transmission, and longitude together explained 67.5% of the variation in oxygen concentrations. In this depth layer, the coefficient for transmission and salinity roughly doubled while that for longitude halved in comparison to the relationship within the entire water column (Table 2). Across all datasets, the relationship between nitrate and volumetric oxygen concentrations executed chemically from bottle casts revealed two separate relationships, one in the cooler waters (<18°C) where oxygen concentrations rose to an asymptote of about 240 μmol L^{-1} at depth (Fig. 8A), and a different relationship above about 18°C where oxygen concentrations decreased linearly with increasing nitrate concentrations. The significant negative correlation between nitrate and oxygen below oxygen concentrations of 222 μmol L^{-1} line suggested a minimum regeneration ratio (O_2 to N) of 10 for the shallowest slope of the curve in Fig. 8A ($r^2 = 0.62$, $n = 21$, $p < 0.01$), but this could reach 20 if the regression were based on the minimum nitrate values in the data envelope used for the regression (Fig. 8A; $r^2 = 0.85$, $n = 33$). A conservative estimate with the highest statistical significance is Nitrate $= -0.0894 \times$ Oxygen + 20.02; $r = -0.9740$; $n = 15$; $p < 0.0001$. This equates to a regeneration rate of 11, or the release of ~0.089 mol N/1 mol O_2 (the Redfield regeneration ratio for phytoplankton would be 6, requiring 0.15 mol N/mol O_2). Between 50 m and 200 m, peak mixed layer nitrate concentrations (~2 μmol L^{-1}) occurred at the lowest oxygen concentrations, at about 20°C (Fig. 8A). Nitrate and phosphate concentrations were linearly correlated throughout the dataset, with a slight drop of the NO_3^-: PO_4^{-3} ratio to ~15.1 in 4 points in deep waters (>30 μmol L^{-1} NO_3^-; data not shown).

The lowest oxygen concentrations (below 193 μmol L^{-1}) occurred at a water density of $\rho = 25.4$–25.5, just below a significant particle peak at a density of $\rho = 24.8$ (Fig. 8B) at temperatures of about 20–21°C, collocated with, but slightly shallower than, the nitrate peak at about 20°C, (Fig. 8A,B). Overall, there was a striking physical coherence between low oxygen and high nitrate concentrations.

Drifter tracks

The three drifter tracks show cycling of the drifters around the eddy center (Fig. 9A–C). Drifter 1, deployed in Period 1 in the LC, well north of the large meander, followed the LC and circled the eddy to the west, coming back toward the coast as the warm LC waters moved shoreward south of the meander at an average speed of 0.9 m s^{-1} and a distance of 150 km from the eddy center (Fig. 9A). Drifter 2a was deployed across Periods 1–2 well within the perimeter of the eddy as defined by the 22° isotherm (Paterson et al. 2008, 2013) and circled the eddy completely once, after which it seemed to be ejected from circulation and rejoined the main body of the LC flowing south (Fig. 9B). This drifter travelled at an average speed of 0.7 m s^{-1} and remained 90 km from the eddy center. It was rescued once it neared the continental shelf, risking running aground (Fig. 9B). In Period 2, Drifter 2b was deployed near the center of the eddy and circled part way around the center at 0.4 m s^{-1} remaining within 10 km of the eddy center (Fig. 9C). It was recovered part-way through execution of the N–S CTD transect.

Multiple linear regression indicated that neither temperature nor salinity showed any statistical change over the time of deployment of Drifter 1 as it followed the LC around the outside of the eddy ($p = 0.85$; $p = 0.73$, respectively). The slight apparent increase in surface salinity would have suggested dilution of LC water by 15% with STW, much lower than the ~33% observed on the SeaSoar2 transect. Oxygen and Chl *a* fluorescence both increased somewhat with time

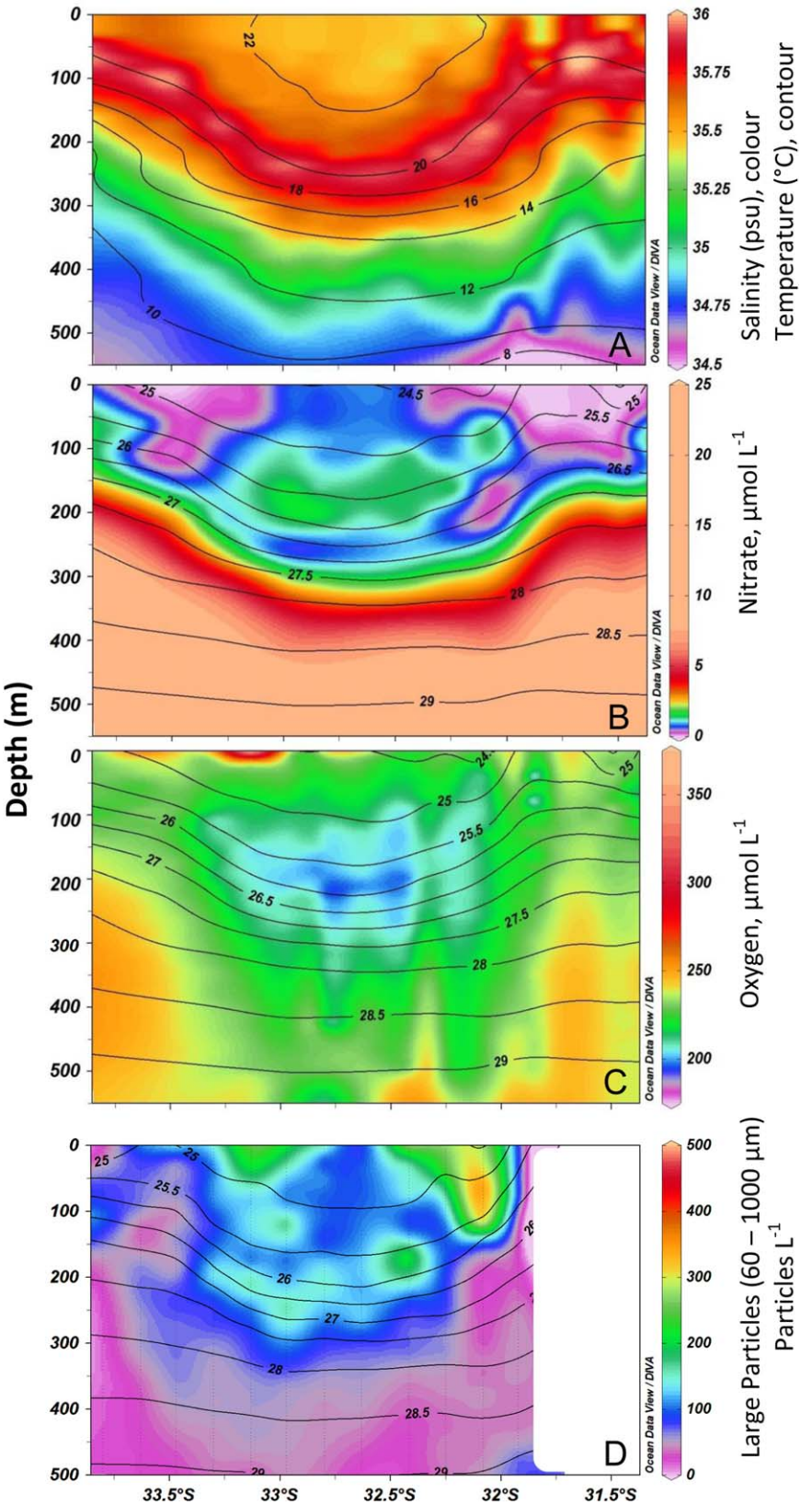

Fig. 7. Regional N–S CTD transect from ~31 to 34 S along ~113.6°E in Period 2 as shown in Fig. 1E. (**A**) Salinity (colour shading) and temperature (black contours). (**B**) Nitrate (colour shading) and density anomaly (black contours). (**C**) Oxygen concentrations in μmol L^{-1}. Note the spatial coherence of nitrate (+) and oxygen (−) between (**B**) and (**C**). (**D**) Large Particulate Matter (0.06–0.53 mm) as measured by the UVP. Note spatial coherence of high LPM and high nitrate and clear peak of particles around 25–25.5 density contour.

Table 2. Multiple linear regressions of oxygen concentration vs. longitude, salinity, and transmission across the study area [O_2] (μmol kg^{-1}) = $C + a$ (longitude, decimal degrees) + b (salinity, psu) + c (% transmission). All three parameters contributed significantly to the regression. Overall, oxygen concentrations were lowest in waters of relatively low salinity, close to shore (with increasing longitude), and higher particle concentrations (decreasing transmission).

Depth range	Linear fit parameters	R^2	N	$p<$*
0–500 m	[O_2] = 1012 − 4.29 (long) − 12.54 (sal) + 1.67 (trans)	0.264	50,104	0.001
50–500 m	[O_2] = 597 − 4.40 (long) − 11.64 (sal) + 5.61 (trans)	0.341	43,994	0.001
150–250 m	[O_2] = 712 − 1.85 (long) − 42.80 (sal) + 13.209 (trans)	0.675	9278	0.001

Note: *All parameters *a*, *b*, and *c* are equally significant ($p < 0.001$) in each multiple regression analysis.

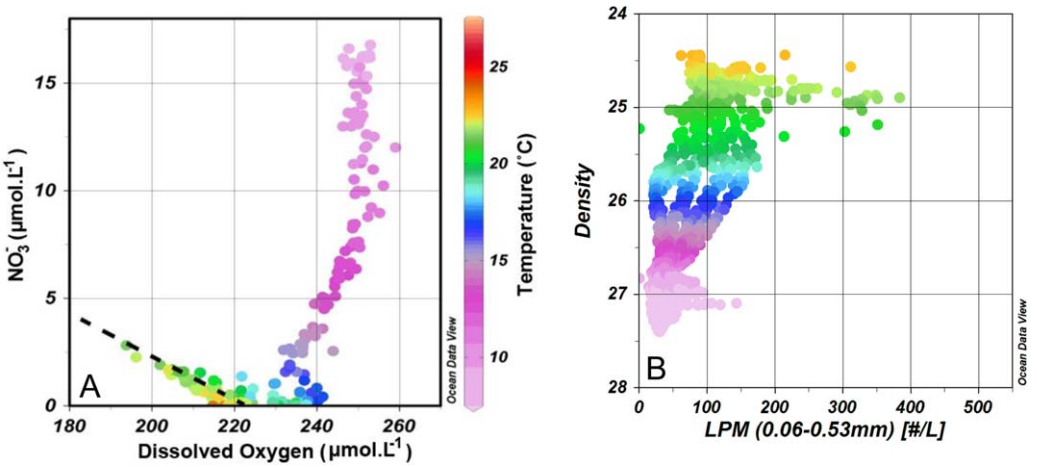

Fig. 8. Relationship between nitrate, oxygen, and temperature (i.e., depth) across the whole dataset. (**A**) Nitrate vs. oxygen, with temperature as symbol colour. Note the relationship between high nitrate and low oxygen at subsaturating oxygen concentrations (below 222 μmol L^{-1}) at relatively high temperatures near the base of the mixed layer. Precise regression slope is sensitive to subjective choice of data subset (see text). (**B**) Large particle (0.06–0.53 mm) concentration from the UVP shows accumulation of particles above the ρ ~25.5 density contour, at ρ ~24.7, and a temperature about 20–21°C also at the base of the mixed layer.

(see below). Nitrate (and silicate, not shown) concentration decreases at the surface (<150 m) were also not significant (Fig. 10, left three panels).

Drifter 2a showed a warming surface layer that deepened as it moved around the inner perimeter of the eddy over 7 d (central panel, top row, Fig. 10). Oxygen concentrations decreased significantly with time, in a layer around and below 150 m depth, with a strengthening mid-depth nitrate maximum ~150 m (Fig. 10 central panel, middle and bottom rows) correlated with similar patterns in silicate (not shown). Over the time period, the oxygen depletion and nitrate accumulation curves appeared to mirror each other to ~200 m (see Table 3), but only oxygen changes with time were statistically significant, estimated via multiple linear regression as a decrease of 1–2 μmol L^{-1} d^{-1}. When integrated vertically, oxygen depletion along the track of Drifter 2a was linear with time ($p<0.05$) at −0.36 mol m^2 d^{-1} (Table 3; see below).

In Period 2, Drifter 2b was deployed near the center of the eddy and circled part way around the center at 0.4 m s^{-1} before it was recovered part-way through execution of the N–S CTD transect. Oxygen and nitrogen concentrations in the eddy center remained steady with time, with oxygen ~20 μmol L^{-1} lower, and nitrate concentrations ~2 μmol L^{-1} higher, relative to measurements along the other drifter tracks (Fig. 10, right panel).

Calculations of biogeochemical impact of the forming eddy

We use the multiple datasets presented here (SeaSoar transects, Drifters, and CTD stations and transects) to calculate the biogeochemical fluxes mediated by eddy activity: (1) offshore fluxes of carbon and Chl *a* in Period 1, and (2) oxygen depletion and nitrate release within the eddy from Period 2. Each dataset yields an estimate with different limitations and potential errors, but each is fully independent (Tables 1, 3).

Offshore fluxes

Closure of the eddy to the coast by 14th May, indicates a period of ~2 weeks during which CW directly entered the eddy center. Strong offshore currents (~0.5 m s^{-1} toward the

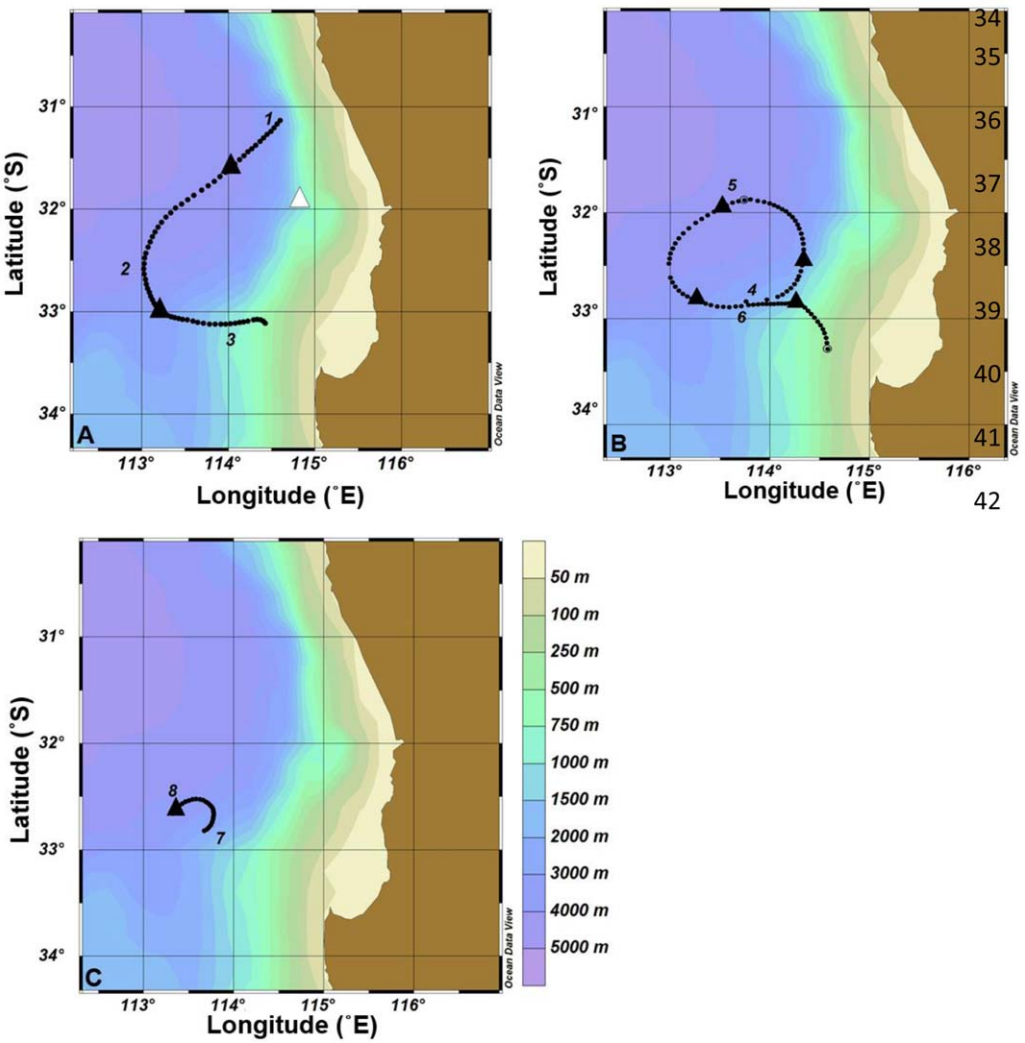

Fig. 9. Tracks of Lagrangian drifters which moved (**A**) around the outside perimeter of the forming eddy (Drifter 1; Period 1) about 150 km from the eddy center at 0.9 m s^{-1}, (**B**) just inside the perimeter of the eddy (Drifter 2a, Periods 1–2) about 90 km from the eddy center at 0.7 m s^{-1} and (**C**) within 10 km of the center of the eddy (Drifter 2b; Period 2) at 0.4 m s^{-1}. Biogeochemical measurements were made every 3 d at stations indicated with consecutive numbers across the three drifters (see Fig. 10). White triangle in 9A indicates position of CW station in Period 1. Depth contours show bathymetry across **A**–**C**.

NW/NNW) carried relatively well-mixed CW into the meander; across the 40 km gap and integrated to 50 m depth this amounts to 2 Sv. The concentrations of POC (51.2 mg m^{-3}) yield a flux estimate of 3.09×10^{10} g of shelf carbon into the eddy over the 2 weeks of eddy formation.

Upstream of the meander, the LC proper crossed the shelf flowing toward the southwest at this time, carrying warmer, fresher water offshore toward the southwest, a flux of about ~4 Sv, then flowing around the outer perimeter of the meander, rejoining the southward flow at the shelf break ~200 km further south. We therefore do not consider the LC per se can mediate net cross-shelf transport, despite significant particle loads within the LC. While CW was injected directly into the eddy (see below), LC waters would have needed to undergo mixing toward the eddy center to contribute their biogeochemical load there. The drifter tracks did not support such mixing; in fact, the ejection of Drifter 2a after one full eddy rotation suggested a slight surface divergence.

Primary production, oxygen depletion, and nitrate release

Integrated primary production rates measured in the euphotic zone across the eddy increased toward the eddy center: Carbon uptake rates were 0.030 mol C m^{-2} d^{-1} in the LC outside the eddy proper (Drifter 1), 0.077 inside the eddy perimeter (Drifter 2a), and 0.104 mol C m^{-2} d^{-1} in the eddy center (Drifter 2b); (Table 3).

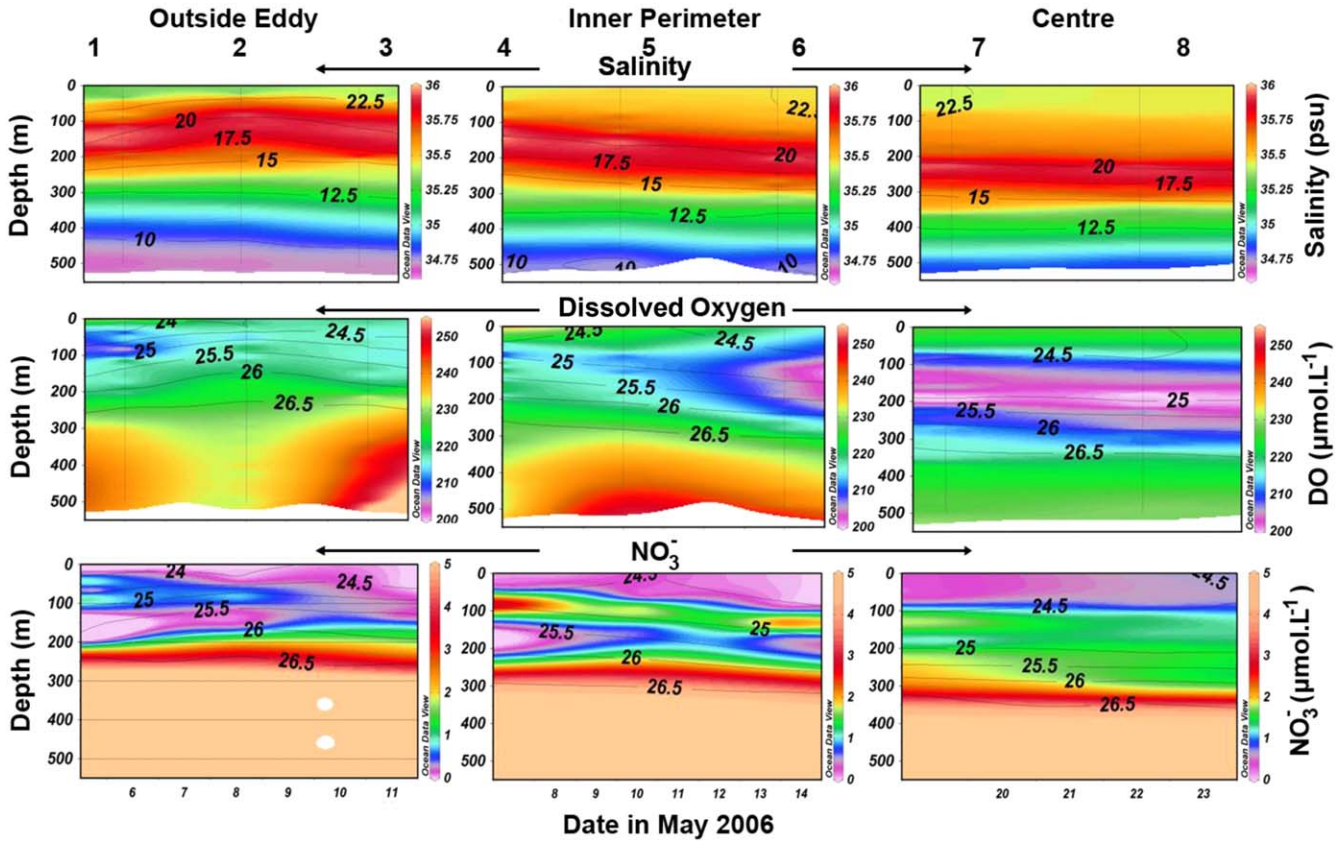

Fig. 10. Time series of physical and chemical properties along the drifter tracks for Drifters 1, 2a, and 2b. **Top 3 Panels**: Salinity (psu), **Middle 3 panels**: Oxygen (μmol L^{-1}), **Bottom 3 panels**: Nitrate (μmol L^{-1}). Left column—Drifter 1, Middle Column—Drifter 2a, and Right column—Drifter 2b. The Leeuwin Current is characterized by high silicate concentrations and low salinity, but there is evidence of progressive mixing with more saline Subtropical Water (35%) with time.

Oxygen depletion and nitrate release between 50 m and 150 m depth were estimated independently from (1) the depth dependent time series of oxygen depletion along each drifter, (2) the difference in integrated oxygen load (per m^2) between offshore and onshore flow along the SeaSoar2 transect, and (3) the difference in integrated oxygen between eddy center and eddy perimeter from the CTD transect. The timeline for (2) was extrapolated from Drifters 1 and 2a, both of which indicated a 7 d rotation period, and the time line for (3) was the 2 week period since eddy isolation (Table 3).

The clearest and best-resolved time line of net oxygen depletion occurred along the track of Drifter 2a moving along the inner perimeter of the eddy (Fig. 10; Table 3). Examined with depth, there were oxygen minima at ~120 m (ca. $\rho = 25.3$–25.5), where higher oxygen depletion rates occurred (up to ~3 mmol m^{-3} d^{-1}), coinciding with net nitrate increases along the drifter track (0.083 mmol m^{-3} d^{-1} and 0.170 mmol m^{-3} d^{-1}). In the euphotic zone there was a net oxygen production ~7.8 mmol m^{-3} over ~1 week (very similar to those estimated via the SeaSoar2 data below, about 1 mmol m^{-3} d^{-1} above the $\rho = 25$ density contour). Drifters 1 (LC) and 2b (Eddy Center) did not show significant oxygen depletion with time, but the difference between them points to a large net oxygen deficit in the eddy center, which is quantified further via the CTD transect data below.

Seasoar2 revealed a doubling of Chl *a* fluorescence in the mixed layer suggesting net growth of phytoplankton over the 1-week rotation period. The depletion of oxygen at depth from ~97% to 90% of saturation amounted to ~10 μmol L^{-1} at ~100 m. Spatially, this depleted layer formed immediately below the first major change in density with depth (the 0.01 $\delta\rho/\delta z$ line in Fig. 6C). The most profound oxygen depletion was centered around the $\rho = 25.4$–25.5 density line, and associated with peak nitrate concentrations (see below), a contour shown to be spatially located immediately below a layer of large particles.

The CTD line along the 113.6°E line transected the eddy center. The lowest vertically integrated oxygen values regionally were found within the eddy center, and the distribution of large particles (60–530 μm, = 0.06–0.53 mm) indicates an apparent accumulation of particles immediately above this

Table 3. Integrated oxygen values pre- and post-eddy, inside the eddy and outside the eddy (Leeuwin Current, LC). Integrations are 50–150 m (SeaSoar) or to 200 m where available. Grey shading indicate estimates of oxygen depletion within the forming eddy; unshaded lines are LC measurements. Numbers in bold show significant depletion with time within the eddy. Estimates increase in uncertainty from top to bottom of the table.

Data source	Integrated O_2 mol O_2 m^{-2} INITIAL → FINAL	O_2 depletion mol O_2 m^{-2} d^{-1}*	Primary productivity mol C m^{-2} d^{-1}	Time and space scale of ΔO_2—measurement or estimate
Lagrangian estimates				
Drifter 1a (LC; outside eddy)	21.5 → 21.8	−0.04 (−0.01)	0.030	to 200 m; 7 d
Drifter 2a (eddy internal perimeter)	22.0 → 20.9	**0.17 (0.35)**	0.077	to 200 m; 7 d Nitrate release 0.17 mmol m^{-3} d^{-1} to 200 m; 3 d
Drifter 2 b (eddy centre)	21.0 → 21.3	−0.10 (−0.03)	0.104	
Eulerian estimates				
SeaSoar 1 (LC, Fig 1B)	NS	NS		to 150 m (spatial)
SeaSoar 2 (Offshore → Onshore; Fig. 1E)	22.8 →21.7	**0.15 (0.19)**		to 150 m (spatial)—Assume 7 d ~rotation of Drifter 2a
CTD transect (cross-eddy; Fig. 1E)	118 → 111 or 118 → 104	**(0.25–1)**		to 500 m (spatial) (perimeter → coast or perimeter → eddy center) Theoretical time line—2 weeks of eddy formation

*[Negative value = release] (Whole water column integration given in brackets where available).

layer. Maximum accumulation of particles of both sizes occurred just above contours of $\rho = 25$, just shallower than the oxygen depletion and nitrate peak at $\rho = 25.4$–25.5. Oxygen depletion to 500 m was about 0.15 mol O_2 m^{-2} d^{-1} (Integrations to 150 m given in Table 3).

Across the whole sampling region, we mapped nitrate along the important $\rho = 25.5$ density contour (Fig. 11A), showing the highest integrated loads near the coast and in a plume moving offshore, with maxima near the eddy center. Particle concentrations across the region were mapped along the same contour, showing offshore maxima also associated with the eddy center (Fig. 11B). Vertically integrated oxygen throughout whole water column showed a remarkable pattern, with oxygen depletion apparently following the historic track of the eddy from the coast to its current center (Fig. 11C).

Discussion

Previous work has identified the potential importance of cross-shelf exchange in fueling the biomass, nutrient, and particle load of large mesoscale eddies of the LC forming at the shelf break off Western Australia (Paterson et al. 2008; Holliday et al. 2011). These eddies are relatively long-lived (9–24 months; Waite et al. 2007b) and can carry heat, salt, momentum, and biogeochemical signatures across large distances throughout the Indian Ocean (Chelton et al. 2011). Here we estimated fluxes of shelf water and associated tracers as they were incorporated into a large anticyclonic feature while it remained physically contiguous with shelf waters. Once isolated from the shelf, we showed that measurable biogeochemical changes within the eddy were rapid (ca. 1 week). These included depletion of oxygen and generation of subsurface nitrate peaks within the eddy. Complete nitrification of organic matter injected from the shelf and upstream LC would contribute significantly to the eddy's productivity budget.

The initiation of the LC meander in late April allowed us to observe the LC meander open to the shelf, with the center of the eddy in direct connectivity with shelf waters during the period of ~2 weeks during which coastal waters directly entered the eddy center. Silicate and nitrate concentrations were typical of shelf-modified LC waters (Holliday et al. 2012) where LC has mixed with STW, and nutrients have been on the shelf long enough to be taken up into Chl *a* (CW) and to be associated with high concentrations of large particles (>300 particles $L^{-1} > 60$ μm). The particles themselves are believed to be a mixture of live plankton and phytodetrital material, but primarily comprised of the latter (Gorsky et al. 2000). The carbon content of the large particles represented about 30% of the total POC (see Guidi et al. 2008) in CW, suggesting that significant amounts of the particulate carbon in coastal waters was either large source particles (such as seagrass or macrophyte wrack) or was planktonic material packaged as aggregates or fecal

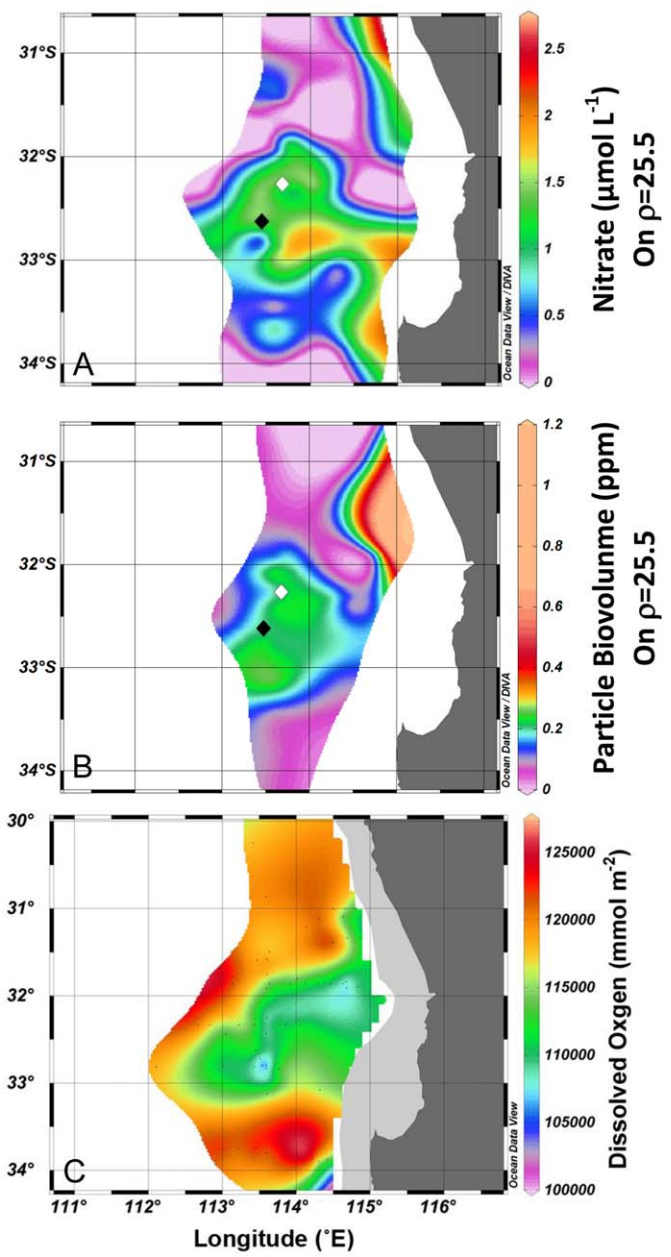

Fig. 11. (**A**) Nitrate across the whole sampling region along the 25.5 density contour. White diamond = eddy center in Period 1, Black diamond = eddy center in Period 2. (**B**) LPM (0.06–0.53 mm) across the whole sampling region along the 25.5 density contour. Diamonds as in 11A. (**C**) Vertically integrated oxygen throughout whole water column.

pellets as the material moved offshore. Strong offshore currents toward the NW carried 2 Sv of CW into the meander; this seaward flux contributed 3×10^{10} g C to the center of the eddy over the ~2 week period of eddy formation. This is of the same order as earlier estimates of the total yearly offshore flux from three eddies over the season (Feng et al. 2007; 4–5 $\times$ 10^{10} g C). Our data therefore suggest a total yearly cross-shelf flux closer to 10×10^{10} g yr^{-1}, about double previous estimates.

It is possible that the LC meander deposited some of its significant particle load (see, for example, Fig. 7D) into the eddy via lateral mixing. Based on salinities (SS1), we estimate that the LC was progressively diluted 16% with STW (lying below the LC) as it moved around the eddy perimeter. However, lateral exchange with the eddy center is more difficult to calculate as the CW contributing most to the eddy core already contains a large fraction of LC water from the shelf. Paterson et al. (2013) showed that the picoplanktonic community in the eddy center was distinct from that in the LC, with a strong salinity boundary around the eddy perimeter, suggesting isolation from the LC on the scale of days. This, and the lack of any measurable convergence in Drifter 1 (LC) or Drifter 2a (eddy internal perimeter) toward the eddy center as they rotated, suggest very limited lateral exchange between the LC and the eddy center (EC).

At the same time that CW was flowing offshore into the eddy center, the LC meander itself was starting to pinch off, with LC waters moving both strongly southward from the north, and northward from the south (see arrows Figs. 3B, 4A), the velocities meeting at a strong velocity front in the center of the offshore flowing CW. The biomass injected into the eddy center was thus isolated from the coast by 14th May, when the southern arm of the meander closed northward near the shelf break. Several independent lines of evidence support the physical isolation of the eddy center from the shelf after this date. SS2 data indicate that a strong velocity front (and biogeochemical front) between the N and S arms of the closed eddy, with offshore flow occurring immediately adjacent to onshore flow, near the shelf break. The quasi-circular tracks of Drifters 2a and 2b, both remaining a constant distance from the eddy center, suggests their physical isolation from the coast. Drifter 2a completed an entire revolution of the eddy and returned to the position where it had been deployed, before being ejected from the eddy. If anything, this latter observation suggests a slight surface divergence of the flow radially outward from the center of the eddy.

The overall picture suggests a productive surface LC water mass (to ~200 m) circling the outer perimeter of the eddy, with waters beneath the euphotic zone not showing major biogeochemical changes with time. In contrast, inside the eddy perimeter the drifter showed a significant deepening of isopycnals with time associated with similar slopes of deepening nitrate and oxygen contours with time. Two possible explanations for this deepening exist—(1) the drifter was moving physically toward the eddy center, or (2) the eddy itself was deepening with time. We favor the latter explanation, given the consistent diameter of the drifter track, and the physical stability of the water column around the outer perimeter. The most significant change along the time series was the overall depletion of oxygen along the drifter track.

The vertically integrated oxygen depletion amounted to 500 mmol m^{-2} d^{-1}, about 80% of which occurred between 100 m and 200 m depth. This was physically associated with net accumulation of 18 mmol NO_3^- m^{-2} d^{-1} in the deep peak (with a plausible ratio of uptake of O_2 to release of NO_3^- there, of 20.7: 1). But a net uptake of 15 mmol NO_3^- m^{-2} d^{-1} occurred between 0 m and 50 m despite net O_2 depletion; simultaneous uptake and release of nitrate in shallow waters would have masked gross nitrate release associated with O_2 depletion closer to the surface.

The eddy center displayed no measurable changes with time in oxygen, nitrate, or physical structure, but its properties (see Fig. 10) suggested that oxygen depletion and associated nitrate release had occurred there since eddy formation. A layer of large particles was spatially contiguous with the coast in the early stages of eddy formation, and were later seen deep within the eddy, physically associated with the oxygen minimum and shallow nitrate peak along the $\rho = 25.5$ density interface; across all datasets the center of the eddy had the most profound oxygen deficit. Overall, then, we used the eddy center as an end point to our calculation of modifications in oxygen and nitrate in time and space. This was summarized further in Table 3 and below.

Could local primary production account for carbon accumulation at the surface that could support the observed rate of oxygen depletion at depth? Our estimates of local carbon uptake rates suggest not. Primary production rates (maximum of 0.10 mol C m^{-2} d^{-1}) simply could not match oxygen depletion observed in the eddy perimeter (0.17–0.35 mol O_2 m^{-2} d^{-1}) or inferred more roughly across the eddy spatially (0.25–1 mol O_2 m^{-2} d^{-1}, see Table 3). Even a very high F-ratio for this system (0.5) would suggest an absolute maximum of 30% of the depletion could be supported by locally produced surface carbon sources.

Our evidence supports the hypothesis that particles sourced from the coast and exported during eddy formation could support subsequent oxygen depletion and nitrate regeneration within the eddy. If the 1×10^{11} g C exported across the shelf over the period of eddy formation were delivered into the eddy center, this would have contributed about 0.01–0.1 mol m^{-2} (for uniform particle delivery across eddy diameters of 200 km vs. 50 km, respectively) to the eddy carbon budget. We therefore conclude that CW injection of particulate matter into the warm core eddy is likely to have contributed about half of the oxygen demand and nitrate release we observed. This highlights the capacity for cross-shelf transport via mesoscale eddies to modify oceanic nutrient budgets, and to contribute significantly to production peaks moving seaward as the eddy matures. As indicated, the estimated potential impact depends critically on assumptions about the eddy diameter across which particles are distributed and/or concentrated as they enter the eddy system.

Regionally, the best predictors of the strength of low oxygen, high dissolved nitrogen layers (LDOHN, *sensu* Thompson et al. 2011) in our study were salinity, turbidity, and longitude. This indicates that there are broader regional sources of variation in oxygen that are oceanographically predictable. We interpret longitude as an effect of distance from shore, for example, suggesting that lowest oxygen concentrations are likely to occur near the coast. Transmission as a predictor would suggest regional association of low oxygen with higher particle concentrations, often maximal near the coast as well as below the LC. The low salinity association is likely to be related to the dynamics of the LC, itself the primary source of lower salinity water regionally. Finally, the marked increase in the correlation coefficient and the parameter estimate at depths between 150 m and 250 m confirms that oxygen depletion is most predictable between the 150 m to 250 m depth interval, and that within this depth interval it is less variable with distance from shore, and more dependent on local salinity and transmission at this depth. In essence, the analysis identifies this depth range as an important location for particle-mediated oxygen draw-down. LDOHN layers are thus largely confined to specific subsurface regions, below the mixed layer and above the deep STW layer, and the association of low salinity waters with particle-rich waters near the coast yields most oxygen depletion regionally at depth. This confirms the role of particle trapping on density surfaces. Eddy dynamics apparently act to focus, isolate and move these LC, and CW-sourced particles offshore.

The depletion of oxygen, and release of nitrate, within the eddy on the timescale of ~2 weeks also suggests a more local source of nitrogen (N) than has recently been proposed for the LC (Thompson et al. 2011); this earlier work suggested that the nitrogen in LDOHN layers could be sourced far upstream, possibly in low latitude waters north of Australia. Our calculations suggest that, based on the estimates of oxygen depletion and time scale of eddy formation, particles carrying the N should originate less than 500 km away. We confirm our earlier conclusion (Waite et al. 2013) that N supply and N turnover are, in fact, very rapid in this system, such that nitrate is acting primarily as a regenerated nutrient in the mixed layer rather than as a source of new nitrogen originating at depth.

References

Baltar, F., J. Arístegui, J. Gasol, I. Lekunberri, and G. Herndl. 2010. Mesoscale eddies: Hotspots of prokaryotic activity and differential community structure in the ocean. ISME J. **4**: 975–988. doi:10.1038/ismej.2010.33

Chelton, D. B., M. G. Schlax, and R. M. Samelson. 2011. Global observations of nonlinear mesoscale eddies. Prog. Oceanogr. **91**: 167–216. doi:10.1016/j.pocean.2011.01.002

Cowen, R. K., J. A. Hare, and M.P. Fahay. 1993. Beyond hydrography—can physical processes explain larval fish

assemblages within the middle atlantic bight. Bull. Mar. Sci. **53**: 567–587.

Cresswell, G. R. 1991. The Leeuwin Current - observations and recent models. Journal of the Royal Society of Western Australia, **74**: 1–14.

Csanady, G. T. 1997. On theories that underlie our understanding of continental shelf circulation. J. Oceanogr. **53**: 207–229.

Feng, M., L. J. Majewski, C. B. Fandry, and A. M. Waite. 2007. Characteristics of two counter-rotating eddies in the Leeuwin Current system off the Western Australian coast. Deep-Sea Res. II, **54**: 961–980.

Feng, M., A. M. Waite, and P. A. Thompson. 2009. Climate variability and ocean production in the Leeuwin Current system of the west coast of Western Australia. J. R. Soc. West. Aust. **92**: 67–81.

Gaughan, D. J. 2007. Potential mechanisms of influence of the Leeuwin Current eddy system on teleost recruitment to the Western Australian continental shelf. Deep-Sea Res. Part 2 Top. Stud. Oceanogr. **54**: 1129–1140. doi:10.1016/j.dsr2.2006.06.005

Gorsky, G., M. Picheral, and L. Stemmann 2000. Use of the underwater video profiler for the study of aggregate dynamics in the North Mediterranean. Estuar. Coast. Shelf Sci. **50**: 121–128. doi:10.1006/ecss.1999.0539

Guidi, L., G. A. Jackson, L. Stemmann, J. C. Miquel, M. Picheral, and G. Gorsky. 2008. Relationship between particle size distribution and flux in the mesopelagic zone. Deep-Sea Res. I., **55**: 1364–1374. doi:10.1016/j.dsr.2008.05.014

Holl, C. M., A. M. Waite, S. Pesant, P. A. Thompson, and J. P. Montoya. 2007. Unicellular diazotrophy as a source of nitrogen to Leeuwin Current coastal eddies. Deep-Sea Research Part II, **54**: 1045–1054. doi:10.1016/j.dsr2.2007.02.002

Heath, M. R. 1992. Field investigations of the early-life stages of marine fish. Adv. Mar. Biol. **28**: 1–174. doi:10.1016/S0065-2881(08)60039-5

Holliday, D., L. E. Beckley, and M. P. Olivar. 2011. Incorporation of larval fishes into a developing anti-cyclonic eddy of the Leeuwin Current off south-western Australia. J. Plankton Res. **33**: 1696–1708. doi:10.1093/plankt/fbr064

Holliday, D., L. E. Beckley, N. Millar, M. P. Olivar, D. Slawinski, M. Feng, and P. A. Thompson. 2012. Larval fish assemblages and particle back-tracking define latitudinal and cross-shelf variability in an eastern Indian Ocean boundary current. Mar. Ecol. Prog. Ser. **460**: 127–144. doi:10.3354/meps09730

Karageorgis, A. P., W. D. Gardner, D. Georgopoulos, A. V. Mishonov, E. Krasakopoulou, and C. Anagnostou. 2008. Particle dynamics in the Eastern Mediterranean Sea: A synthesis based on light transmission, PMC, and POC archives (1991-2001). Deep-Sea Res. Part I. **55**: 177–202. doi:10.1016/j.dsr.2007.11.002

Ladd, C., W. R. Crawford, C. E. Harpold, W. K. Johnson, N. B. Kachel, P. J. Stabeno, and F. Whitney. 2009. A synoptic survey of young mesoscale eddies in the Eastern Gulf of Alaska. Deep-Sea Res. Part 2 Top. Stud. Oceanogr. **56**: 2460–2473. doi:10.1016/j.dsr2.2009.02.007

Mackas, D., M. Tsurumi, M. Galbraith, and D. Yelland. 2005. Zooplankton distribution and dynamics in a North Pacific Eddy of coastal origin. II. Mechanisms of eddy colonization by and retention of offshore species. Deep-Sea Res. II. **52**: 1001–1035. doi:10.1016/j.dsr2.2005.02.008

Montoya, J. P., M. Voss, P. Kaehler, and D. G. Capone. 1996. A simple, high precision tracer assay for dinitrogen fixation. Applied and Environmental Microbiology, **62**: 986–993.

Myers, R. A., and K. Drinkwater. 1989. The influence of gulfstream warm core rings on recruitment of fish in the Northwest Atlantic. J. Mar. Res. **47**: 635–656. doi:10.1357/002224089785076208

Nakata, H., S. Kimura, Y. Okazaki, and A. Kasai. 2000. Implications of meso-scale eddies caused by frontal disturbances of the Kuroshio Current for anchovy recruitment. Ices Journal of Marine Science, **57**: 143–151. doi:10.1006/jmsc.1999.0565

Nodder, S. D., and A. M. Waite. 2001. Is Southern Ocean organic carbon and biogenic silica export enhanced by iron-stimulated increases in biological production? Sediment trap results from SOIREE. Deep-Sea Res. Part II. **48**: 2681–2701. doi:10.1016/S0967-0645(01)00014-5

Nodder, S. D., M. A. Charette, A. M. Waite, T. W. Trull, P. W. Boyd, J. Zeldis, and K. O. Buesseler. 2001. Particle transformations and export flux during an in situ iron-stimulated algal bloom in the Southern Ocean. Geophys. Res. Lett. **28**: 2409–2412. doi:10.1029/2001GL013008

Painter, S. C., R. E. Pidcock, and J. T. Allen. 2010. A mesoscale eddy driving spatial and temporal heterogeneity in the productivity of the euphotic zone of the northeast Atlantic. Deep-Sea Res. Part II. **57**: 1281–1292. doi:10.1016/j.dsr2.2010.01.005

Parsons, T. R., Y. Maita, and C. M. Lalli. 1984. Manual of chemical and biological methods for seawater analysis. Pergamon.

Paterson, H. L., M. Feng, A. M. Waite, D. Gomis, L. E. Beckley, D. Holliday, and P. A. Thompson. 2008. Physical and chemical signatures of a developing anticyclonic eddy in the Leeuwin Current, eastern Indian Ocean. J. Geophys. Res. Oceans **113**. doi:10.1029/2007JC004707

Paterson, H., K. Heel, and A. Waite. 2013. A warm-core eddy linking shelf, Leeuwin Current and oceanic waters demonstrated by near-shelf distribution patterns of Synechococcus spp. and Prochlorococcus spp. in the eastern Indian Ocean. Mar. Freshw. Res. **64**: 1011–1021. doi:10.1071/MF12271

Picheral, M., L. Guidi, L. Stemmann, D. M. Karl, G. Iddaoud, and G. Gorsky. 2010. The Underwater Vision Profiler 5:

An advanced instrument for high spatial resolution studies of particle size spectra and zooplankton. Limnol. Oceanogr.: Methods **8**: 462–473. doi:10.4319/lom.2010.8.462

Rodriguez, J., and others. 2001. Mesoscale vertical motion and the size structure of phytoplankton in the ocean. Nature **410**: 360–363. doi:10.1038/35066560

Thompson, P. A., S. Pesant, and A. M. Waite. 2007. Contrasting the vertical differences in the phytoplankton biology of a dipole pair of eddies in the south-eastern Indian Ocean. Deep-Sea Research Part II, **54**: 1003–1028. doi: 10.1016/j.dsr2.2006.12.009

Waite, A., and others. 2007a. Food web structure in two counter-rotating eddies based on [delta] 15N and [delta] 13C isotopic analyses. Deep-Sea Res. Part 2 Top. Stud. Oceanogr. **54**: 1055–1075. doi:10.1016/j.dsr2.2006.12.010

Waite, A. M., S. Pesant, D. A. Griffin, P. A. Thompson, and C. M. Holl. 2007b. Oceanography, primary production and dissolved inorganic nitrogen uptake in two Leeuwin Current eddies. Deep-Sea Res. Part 2 Top. Stud. Oceanogr. **54**: 981–1002. doi:10.1016/j.dsr2.2007.03.001

Waite, A. M., V. Rossi, M. Roughan, B. Tilbrook, P. A. Thompson, M. Feng, A. S. J. Wyatt, and E. J. Raes. 2013. Formation and maintenance of high-nitrate, low pH layers in the eastern Indian Ocean and the role of nitrogen fixation. Biogeosciences **10**: 5691–5702, doi:10.5194/bg-10-5691-2013.

Werner, F. E., and J. A. Quinlan. 2002. Fluctuations in marine populations: Physical processes and numerical modelling. ICES Mar. Sci. Symposia **215**: 264–278.

Wood, E. D., F. A. J. Armstrong, and F. A. Richards. 1967. Determination of nitrate in sea water by cadmium-copper reduction to nitrite. Journal of the Marine Biological Association of the United Kingdom, **47**: 23–31.

Acknowledgements

We thank D. Krikke for logistic and laboratory support, the captain and crew of the R.V. Southern Surveyor for expert assistance at sea, and the Australian National Marine Facility for ship-time granted for this project. JPL is currently an American Association for the Advancement of Science (AAAS) Overseas Fellow serving at the United States Agency for International Development. This article was a collaboration with JPL in his personal capacity, and is the result of the author's independent research. The opinions and views expressed in this article are the author's own and do not necessarily represent the views of AAAS, or the U.S. Agency for International Development or the United States Government.

Submitted 13 March 2015
Revised 22 July 2015
Accepted 28 August 2015

Associate editor: Susanne Menden-Deuer